# Damage onset analysis of optimized shape memory polymer composites during programming into curved shapes

K.D.C. Emmanuel [a,b], L.H.J. Jeewantha [a,b], H.M.C.M. Herath [c], J.A. Epaarachchi [a,b *], T. Aravinthan [a,b]

[a] School of Mechanical and Electrical Engineering, Faculty of Health Engineering and Sciences, University of Southern Queensland, Toowoomba, Australia

[b] Centre for Future Materials, University of Southern Queensland, Toowoomba, Australia

[c] Department of Engineering Technology, Faculty of Technological Studies, Uva Wellassa University, Badulla, Sri Lanka

[*] Corresponding author:

**J.A. Epaarachchi**

School of Mechanical and Electrical Engineering, Faculty of Health Engineering and Sciences, University of Southern Queensland, West Street, Toowoomba, QLD 4350, Australia.

Email: Jayantha.Epaarachchi@usq.edu.au

**Keywords:**

Shape memory polymer composites, Damage, Effective programming, Parametric optimization, Thickness effects, FEA damage prediction

**Abstract**

The unique shape memorizing ability of shape memory polymers (SMPs) and their fibre reinforced composites have offered the prospect of remedying challenging, unsolved engineering applications. Interestingly, research integrating deformable shape memory polymer composites (SMPCs) in prefabricated modular constructions, deployable outer space structures and other compactable structural components have emerged in the recent past. To ensure effective use in strength demanding applications, SMPC components must possess better mechanical properties. Increased fibre content in SMPCs will improve mechanical properties but can adversely affect the shape memory effect (SME), increasing the possibility of material damage when programming into curved shapes and bends. This will degrade the strength capacity of SMPCs in their applications. This paper details a complete study performed on this critical effect optimizing SMPC properties by means of a 3x3 Taguchi array. The study also provides an experimental framework demonstrating how these undesirable effects can be mitigated coupled with an ABAQUS finite element analysis (FEA) damage prediction strategy. Interestingly, the compression side of the specimen was found to be the most critical location prone to programming damage. In addition, a compressive stress level of 70 MPa was found to be the damage onset stress ($\sigma_o$) point for programming using FEA, and correlated with experimental results. The proposed experimental and FEA framework will enhance future SMPC component design, allowing researchers to predict the possibility of programming damage numerically, saving time and cost. We believe that these findings will aid researchers seeking to develop strong and efficient functional SMPCs for future engineering applications.

## 1. Introduction

The shape memory polymer (SMP) is a functional stimuli responsive smart material with an excellent ability to memorize its original shape. When exposed to an external stimulus such as heat, electricity, light or moisture, SMP matrix softens, allowing deformation into a temporary shape [1, 2]. This smart material has the capability of holding its deformed shape until the respective stimulus is reapplied to initiate shape recovery [3]. In the SMP research context, the process of deforming a SMP into a temporary shape is often known as shape programming or training.

Even though SMPs have distinctive properties compared to traditional materials, inherent poor mechanical properties has been their major weakness [4]. Consequently, different types of fillers and fibre reinforcements were integrated with the SMP matrix to enhance mechanical properties [5-7]. The matrix binds these fillers and fibre reinforcements together and distributes induced stresses through the whole shape memory polymer composite (SMPC). Particulate fillers such as graphene oxide (GO) [8], multi walled carbon nanotubes (MWCNT) [9], carbon black (CB) [10] and rare earth organic fillers [11] produce thermal [8], electrical [9, 10] and photothermal [11] property enhancements, and fibre reinforcements improve structural properties such as resistance to cyclic loading [12], modulus, stiffness and strength [5]. SMPC hinges [13], truss booms [14], solar arrays [13], reflector antennas [15, 16], morphing structures [17, 18] and mandrels [19] are a few of the renowned applications proposed for SMPCs.

Prefabricated modular construction is an emerging modern construction technology developed by researchers and engineers to offer faster and efficient building constructions. This new trend in construction has become a game changer for extremely challenging constructions in overly congested cities where space is limited and time is critical. Compared to traditional construction methods, it offers safer manufacturing, faster construction speeds, better quality control, fewer workers on site, less resource wastage and a smaller environmental impact [20]. Importantly, in prefabricated constructions, different modules of a building are manufactured in a factory and transported to the construction site. These prefabricated modules are then stacked on top of each other to construct a building using cranes. Despite their exciting benefits, difficulties in the transportation and handling of heavy large sized modules is a major drawback in modular construction [21]. Alternatively, researchers have demonstrated the ability of polymer composite materials to mitigate the heaviness of steel prefabricated modules [20].

Excitingly, SMPCs are a competent substitute material for general polymer composites as they possess a temporary shape changing ability. Thus, light weight modules prefabricated with SMPCs can be heated and deformed to a compact shape in factory for easy transportation. SMPC modules can then be heated on-site to recover the initial shape and construct the building. Hence, the integration of SMPCs into structural components, panels, etc. promotes easy transportation and handling, thus mitigating the current drawbacks of prefabricated modular construction. Consequently, these SMPC components must be deformed into curves and bends at multiple locations to achieve compact shapes. Thus, this paper mainly aims to study the effectiveness of SMPCs during programming into such curves and bends. Further, these compactable SMPC integrated components can also be used for emerging concepts such as deployable structures for space habitats which can be used for space exploration [22].

Having sufficient mechanical properties such as tensile and compressive strengths is mandatory for SMPC components. Increasing the fibre content in the composite improves its mechanical properties and, as a consequence, the thickness of the composite is increased. However, the increase in thickness and fibre content causes local damage, fibre buckling and delamination during shape programming procedures. To the author’s knowledge, significant research work investigating the adverse effects of SMPCs with high thickness and fibre content has not yet been conducted. In addition, the identification of damage onset stress and development of a constitutive approach to predict possible damage numerically have not been studied. However, some research on fibre buckling during flexural strains was carried out by Lan et al for a low thickness (2 mm) and small scaled SMPC sample (length = 30 mm and width = 5 mm) under high deformation curvature with low deflection (~ 0.4 mm) [23]. In addition, Gall et al investigated the phenomenon of material damage during programming of a 0.3 mm thick prepreg SMPC, concluding that out of plane fibre buckling and delamination must be avoided for successful shape training. The selection of suitable fibre weave architecture, resin system and tow spacing were suggested as possible solutions to mitigate undesirable thickness effects [24], but the adverse effects on mechanical properties and ways to predict damage by any means were not investigated. Interestingly, recent studies by Gu et al have proposed theoretical modelling techniques for the SME of unidirectional continuous carbon fibre SMPCs. They were based on thermodynamics with internal state variables and refined sinusoidal shear deformation plate theory, but requires a series of verification experiments to adequately prove the validity and accuracy of the models.  [25, 26].

Our research was conducted for epoxy based, large scale SMPCs reinforced with glass, carbon and basalt fibre. A 3x3 (L9) Taguchi array was developed considering the identified parameters to study material damage and come up with the optimal material constituent combination for large scaled samples under high deflection (15 mm). In addition, a new user-friendly damage quantifier was introduced to evaluate and compare damage levels of the programmed SMPCs. Refinements in the fibre orientation and programming process were implemented and tested to obtain zero areal damage percentage (ADP %) and resulted in a zero drop in tensile strength after programming and recovery. Additionally, $\sigma_o$ and critical stress margins (CSM) for flawless programming of the optimized SMPC were proposed via ABAQUS finite element analysis (FEA) which can facilitate prompt prediction of damage and critical locations. Furthermore, experimental outcomes were validated via the developed FEA numerical approach. The outcomes of the research provide firsthand knowledge and an experimental framework coupled with FEA for future researchers to develop high strength SMPC structural components for future constructions.

## 2. Materials and methods

### 2.1 Materials

In this study, an epoxy based SMP was used by mixing two selected amine based hardeners with the epoxy resin in a predefined weight ratio to facilitate a stoichiometric chemical reaction. Amine based Aradur HY 951 (Triethylenetetramine) and Jeffamine D230 were used as hardeners with commercially available Bisphenol-A epoxy based resin Araldite GY 191. Evaluation of the mixing ratio of these chemicals was inspired by a previously published article [27] and, to avoid repetition, respective results and analysis have not been presented here. Thus, the selected chemical mix ratio (by weight) of GY 191 : HY 951 : D230 was evaluated as 13.03 : 1.00 : 1.63.

SMPCs were fabricated by integrating 200 gsm plain weave glass, basalt and carbon fibre fabrics as primary reinforcements. In addition, for second stage optimizing, a stitched unidirectional glass fibre fabric of areal density 500 gsm was used for reinforcement refinements to resolve recognized defects.

### 2.2 Application of Taguchi method for SMPC optimization

Once the chemical composition was selected, a Taguchi array was introduced with identified parameters as a statistical approach to decide on thickness effects on the desired properties and their limitations. The Taguchi method is a robust design method frequently used in engineering applications, particularly to identify optimal process parameters by reducing the number of tests to be conducted. Table 1 illustrates the 3 x 3 experimental design with three identified parameters or factors: (1) fibre type, (2) thickness and (3) number of reinforcement layers. Selected levels of each factor are also given in Table 1.

*Table 1: Selected test parameters and levels*

| Factors | | Levels | | |
|---|---|---|---|---|
| | | **1** | **2** | **3** |
| **1** | Fibre type | Basalt | Glass | Carbon |
| **2** | Thickness (mm) | 3 | 4 | 5 |
| **3** | Number of reinforcement layers | 6 | 8 | 10 |

*Table 2: Developed L9 Taguchi array*

| Specimen (SP) | Fibre type | Thickness (mm) | Number of reinforcement layers |
|---|---|---|---|
| **1** | | 3 | 6 |
| **2** | Basalt | 4 | 8 |
| **3** | | 5 | 10 |
| **4** | | 3 | 8 |
| **5** | Glass | 4 | 10 |
| **6** | | 5 | 6 |
| **7** | | 3 | 10 |
| **8** | Carbon | 4 | 6 |
| **9** | | 5 | 8 |

According to Table 2, nine SMPC samples were fabricated with respective thicknesses, reinforcement type and number of layers. A mold with two glass plates of size 400 mm x 400 mm was used with five steel spacers of the required thickness. The sides were properly sealed with silicone to avoid polymer leaks. Once the mold was ready, the three chemicals were mixed in the selected weight ratio. Then, the SMP was degassed in a vacuum for 15 min at room temperature and poured into the mold. After curing for 24 h at room temperature, post curing was done at 100 ºC for 1.5 h and 130 ºC for 1 h [27]. Finally, the SMPC sheet was demolded and cut into standard test sizes using a waterjet. Fibre mass fractions (w/w %) of SMPCs were evaluated with burnout tests and the results are given in Table 3.

*Table 3: Fibre mass fractions of specimens*

| Specimen (SP) | Fibre mass fraction (w/w %) |
|---|---|
| 1 | 29.4 |
| 2 | 28.7 |
| 3 | 28.8 |
| 4 | 48.3 |
| 5 | 47.0 |
| 6 | 25.3 |
| 7 | 38.2 |
| 8 | 19.0 |
| 9 | 20.7 |

### 2.3 Dynamic mechanical analysis (DMA)

Storage onset temperature (Ts) and Tan δ peak temperature ($T_\delta$) of materials were evaluated using TA Instruments HR-2 Discovery Hybrid Rheometer with a dual cantilever fixture. 8 x 45 $mm^2$ sized samples were used to characterize the storage modulus by means of an Oscillation (temperature ramp) mode. A displacement of 25 μm was applied at a frequency of 1 Hz. During the test, samples were heated from 20 ºC to 120 ºC with a temperature ramp of 5 ºC/min.

### 2.4 Tensile and compression tests

The SMPC's tensile and compressive mechanical properties were investigated according to standard testing procedures using MTS 100 kN testing apparatus. Testing standards ISO 527-4:2009 and ASTM D6641/D6641M – 16 were used for tensile and compressive tests, respectively.

### 2.5 Shape memory effect (SME) test

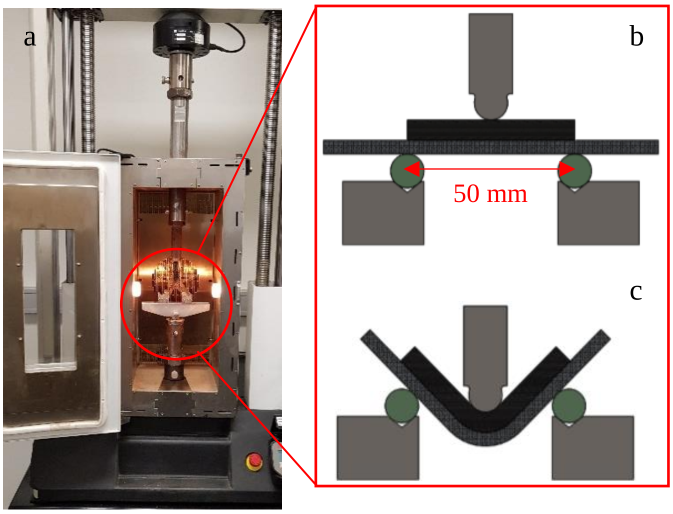


*Figure 1: (a) Experimental setup (b) Initial shape of the sample (c) Programmed shape*

Shape memory properties and the performance of selected SMPCs were studied and analyzed in terms of fixity ratio ($R_f$), recovery ratio ($R_r$) and APD %. Samples of size 100 mm x 20 mm were used to evaluate the SME characteristics of each SMPC. The thermo-mechanical cycles of SMPCs were implemented in MTS 10 kN testing machine along with its compatible thermal chamber as shown in Figure 1. Programming of SMPCs were carried out at two temperatures: $T_S$ and $T_\delta$. First, a sample was placed on the bending fixture with a support span of 50 mm and was allowed to heat up to its programming temperature for 30 min. Then, the programming stage was initiated with two selected deformation rates: (1) 1 mm/min and (2) 60 mm/min. Each SMPC was deformed bending up to a depth of 15 mm at the center of its span. A piece of rubber of size 50 x 25 x 6 $mm^3$ was placed on the top face of the SMPC during programming to increase bend radius and minimize stress concentration. After programming, the thermal chamber was switched off allowing the sample to cool down to room temperature. The sample was cooled for 30 min with the thermal chamber door open to facilitate accelerated cooling. The force applied on the SMPC was maintained throughout the cooling process. Once the sample has properly cooled, force was released to obtain the fixed temporary shape. Then, the deformed SMPC was placed in an oven set to its $T_\delta$ for 15 min to recover initial shape. During this testing procedure, photographs of the programmed, fixed and recovered shapes were taken using a camera and microscope.

## 2.6 Damage analysis

Damage levels of the tested SMPCs were quantitatively analyzed in a macro scaled perspective to identify optimum material parameters. Scanning electron microscope (SEM) is a well-known instrument used for the inspection of materials. However, SEM can only be carried out for a very small part of the sample. In addition, tedious SEM sample preparation requires specialized equipment and the process of cutting a tiny test piece from the damaged area can further damage and distort the SMPC, thus affecting the reliability of test results. Hence, the proposed user-friendly technique enables quick and reliable damage analysis of the programmed SMPC. The side view of the bent SMPC was used for the analysis as it displays the through thickness behaviour of the material due to induced stresses while bending. Thus, a dimensionless quantity ADP % has been introduced to assess samples through thickness damage levels. The ADP % given in Eq. (1) compares the ratio of the damaged area ($A_D$) to the total deformed area ($A_T$). Figure 2 shows: (a) the programmed shape of SP-1 at $T_\delta$ (~ 84 °C), (b) total deformed area ($A_T$) and (c) damaged area ($A_D$). ADP % values were evaluated by measuring $A_T$ and $A_D$ values using the measure tool in SolidWorks.

$$\text{ADP } \% = \frac{A_D}{A_T} \times 100\% \qquad (1)$$

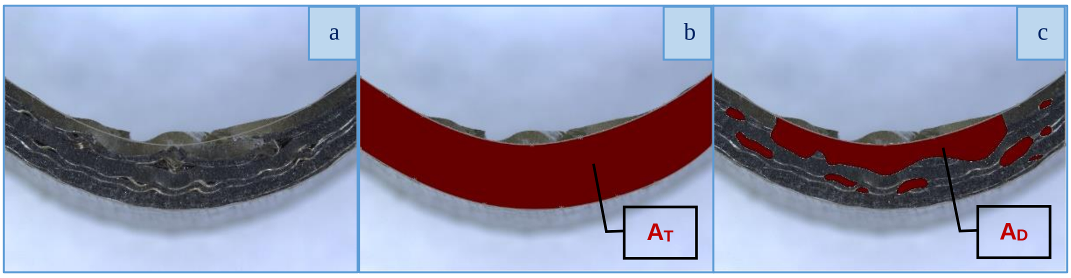


*Figure 2: (a) Programmed shape (b) Total deformed area (c) Damaged area*

**2.7 FEA analysis**

The programming stage was simulated in ABAQUS FEA software to analyze the stress distribution within the sample. As SMP/SMPC programming takes place within the transition region, the material will have a mix of both elastic and viscous properties. Hence, the programming step was defined as a "visco" step with "viscoelastic" material property which was previously studied by Azzawi et al (2017) [28]. As suggested, Prony series relaxation data extracted from DMA Q800 were used to define the viscoelastic properties of the material. In addition, tensile properties at the programming temperature are required to define SMPC material properties. The experimental programming test was simulated in ABAQUS for a SMPC of size 100 mm x 20 mm x 3 mm.

## 3. Results and discussion

### 3.1 Material properties

#### 3.1.1 Dynamic Mechanical Analysis (DMA)

For SMPCs to be used in the structural components of modular constructions, having a $T_g$ higher than average environmental temperature is mandatory. In addition, SMPC properties start dropping when heated beyond $T_g$. Thus, the $T_g$ of a SMP is one of the key characteristics which outline a material's performance range and limitations. Therefore, DMA tests were carried out to identify this critical temperature value.

In the SMP context, $T_g$ is also referred to as the temperature at which both programming and recovery are undertaken. However, the definition of Tg is not certain among SMP research. In general, for all one way SMPs, the higher the temperature of the sample, the easier the programming. Conversely, programming at higher temperatures is not always favourable due to a higher consumption of energy and time. Thus, research suggests that SMP shape training can be categorized into different temperature ranges as cold (below $T_S$), warm ($T_S$ to $T_\delta$) and hot programming (above $T_\delta$) [29, 30]. Feldkamp et al investigated the effect of deformation temperature on the ultimate deformation strain ($\varepsilon_{UL}$) of an epoxy shape memory pristine polymer under tension and concluded that $\varepsilon_{UL}$ can be increased 3 to 5 folds at $T_S$ [31]. Hence, $T_S$ and $T_\delta$ which lie within the borders of the warm temperature region were selected for this study. Figure 3 shows the characterization of the storage modulus and Tan δ of SP-1. The transition values $T_S$ and $T_\delta$ of SP-1 were found to be 58 ºC and 83.8 ºC, respectively. According to Table 4, it can be seen that respective transition temperatures have changed with the specimen constituents. This suggests that SMPC's thermomechanical characteristics depend on material composition defined by their thickness, fibre type and number of reinforcement layers.

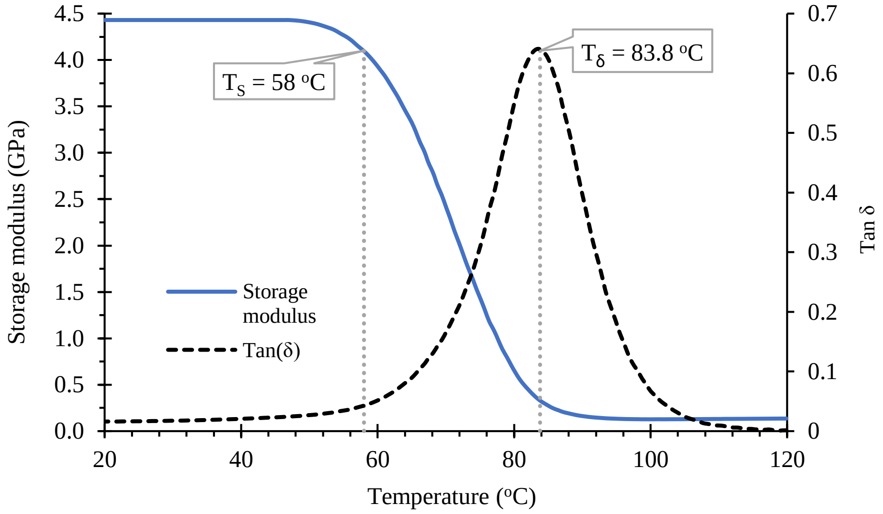


*Figure 3: DMA results characterizing the storage modulus and Tan $\delta$ of SP-1*

*Table 4: Transition temperatures of samples*

| **Specimen (SP)** | **$T_S$ (°C)** | **$T_\delta$ (°C)** |
|---|---|---|
| 1 | 57.6 | 83.8 |
| 2 | 59.7 | 86.9 |
| 3 | 57.6 | 88.4 |
| 4 | 60.0 | 81.9 |
| 5 | 55.4 | 82.5 |
| 6 | 58.9 | 85.9 |
| 7 | 59.5 | 83.9 |
| 8 | 53.2 | 84.7 |
| 9 | 59.4 | 85.2 |

## 3.2 L9 Taguchi analysis

### 3.2.1 Shape memory and mechanical properties

- **Shape fixity and recovery ratios**

Shape memory performance of SMPs is commonly studied in terms of $R_f$ and $R_r$ [32-34]. The $R_f$ shows the extent to which a material can hold its deformed shape when the external force is removed, while $R_r$ relates to the amount of shape recovered. The study of these shape memory parameters is vital in proposed SMPC applications. That is, deformed SMPC structural components produced in factories should be capable of retaining their deformed shape during transportation to construction sites. Then, upon heating on-site, maximum recovery is expected for module assembling. Hence, these crucial parameters of the developed test samples were measured and analyzed to achieve maximum shape memory performance of the optimized material.

Table 5 provides the evaluated $R_f$ % and $R_r$ % values of all nine SMPC specimens. During SME testing, some samples experienced cracking, with fibre damage mostly at the lower temperature $T_S$ (given by "X"). The reasons for such phenomenon and other possible damage types are discussed in the "damage analysis" section of this article. At a given temperature (as in Table 5), evaluated values are different to one another and it is evident that material composition defined by the thickness, fibre type and fibre content has affected shape memory performance despite having the same polymer matrix. This can be attributed to the changes in fibre matrix bond characteristics, reinforcement mechanical properties and bending stress distribution through the thickness. In addition, higher $R_f$ % and $R_r$ % values were obtained at the higher temperature $T_\delta$ compared to $T_S$. This is due to a high loss of material stiffness as the material approaches the rubbery phase [35], allowing the material to store more strain energy when deformed. However, programming at higher temperatures caused material defects in SMPC specimens, which is a significant drawback in terms of SMPC material performance and application.

*Table 5: Fixity and recovery ratios of samples at two selected transition temperatures*

| **Specimen (SP)** | **Programming** | | | |
|---|---|---|---|---|
| | **At $T_S$ (ºC)** | | **At $T_\delta$ (ºC)** | |
| | **$R_f$ %** | **$R_r$ %** | **$R_f$ %** | **$R_r$ %** |
| 1 | 91.7 | 93.0 | 99.0 | 95.4 |
| 2 | X | X | 95.3 | 96.9 |
| 3 | X | X | 96.7 | 97.3 |
| 4 | 91.4 | 90.4 | 95.8 | 91.5 |
| 5 | 96.4 | 86.4 | 79.2 | 90.6 |
| 6 | X | X | 92.9 | 92.6 |
| 7 | X | X | 86.2 | 95.2 |
| 8 | X | X | 93.9 | 94.7 |
| 9 | X | X | X | X |

- **Mechanical properties of SMPCs**

Superior shape memory properties alone cannot transform SMPCs highly competent compared to traditional materials. Having adequate mechanical properties is a vital factor for SMPCs to outrace performance of other common materials in construction engineering applications. Consequently, the SMPC tensile and compressive properties were analyzed and considered as output variables of the Taguchi L9 analysis. Figure 4(a) shows the tensile properties of the test samples in terms of tensile strength and elastic modulus. Among all test samples, carbon fibre reinforced SMPCs showed the best tensile properties due to the superior material properties of the carbon fibre reinforcement [22]. However, basalt SMPCs have almost the same tensile properties as glass fibre SMPCs, even with comparatively low fibre fractions. This is due to the better structural properties of the basalt fibre compared to E-glass reinforcement [36]. A slight variation among the tensile values of basalt SMPCs can be seen due to almost similar fibre weight fractions (29.4 %, 28.7 % and 28.8 %). Moreover, SP-4 and SP-5 with the highest fibre weight fraction of the glass samples have similar tensile properties, while SP-6 with the lowest fibre content of 25.3 % showed the weakest properties. Interestingly, both tensile strength and elastic modulus showed a similar trend and demonstrated a proportional relationship between tensile characteristics and fibre content.

The variation in compressive strength and moduli of test samples are illustrated in Figure 4(b). Compared to tensile properties, carbon fibre SMPCs did not show a significant improvement under compressive loading with respect to other reinforcements. However, as in tensile properties, an almost identical trend can be seen between compressive strength and its modulus. Thus, these results agree with the claim that an increase in fibre content (or fraction) results in the enhancement of the SMPC's mechanical properties [37]. Most importantly, evaluated tensile and compressive properties of the specimens have shown better mechanical properties and structural capability compared to structural characteristics of other previously studied SMPCs [38, 39], exhibiting their potential to be integrated in deformable structural components.

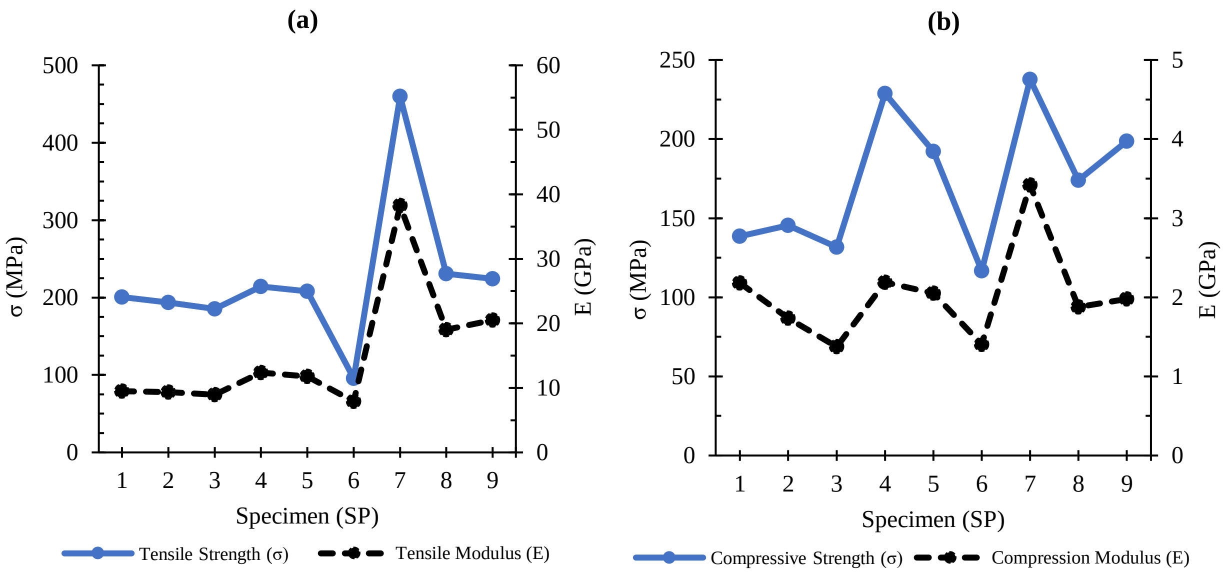


*Figure 4: Mechanical properties of SMPC specimens. (a) Tensile and (b) Compressive material properties*

### 3.2.2 Damage analysis

The SME of a shape memory material makes it distinct and effective compared to traditional materials. Hence, the SME of these functional materials should be flawless to be used effectively in challenging applications. The SMPs and their composites are expected to deform at a suitable transition temperature under the applied load, leaving no damage to the shape memory component. Such undesirable damage during programming can result in the weakening of SMPC components.

During the shape training process, the heated SMP will be in a flexible but weak rubbery state due to matrix softening and degradation [40]. Hence, the matrix-fibre interface which supports fibres and engages in stress transfer when loaded, will be weakened [41-43]. Consequently, the interfacial bond strength between matrix and fibre will be in a weak state during programming. In addition, the failure mode and strength capacity of the polymer composite will rely on the interfacial bond strength [41, 44] which is a crucial factor for SMPC programming. Interestingly, the stress at the onset of damage has been introduced as a measure of interfacial bond strength of the composite [41]. Hence, even reinforced SMPCs might not have enough strength to withstand the deformation strain levels. In such cases, the material is prone to damage due to deformation strains induced whilst programming. In addition, these undesirable effects become prominent as the material thickness increases. Hence, the investigation of material damage in the programming stage of SMPCs is vital to develop versatile future smart components.

According to the results, thicker SMPC samples with high fibre volume fraction resulted in high damage levels. Specially, irrespective of the temperature, carbon SMPCs have shown weakest programmability due to high stiffness. This is due to significant improvement gained in stiffness and other mechanical properties by carbon fibre integration compared to other fibre types.

Even though most of the samples cracked with severe material damage at $T_S$, few glass and basalt SMPCs displaced significantly low ADP % values. The damage levels of the specimens SP-1, SP-4 and SP-5 which performed best during the programming process with better damage resistance are presented in Figure 5 for comparison. Hence, $T_S$ can be concluded as the best transition temperature to program SMPCs to minimize possible material damage. This was also suggested by Feldkamp et al [31] for a neat flexible SMP under tensile loading.

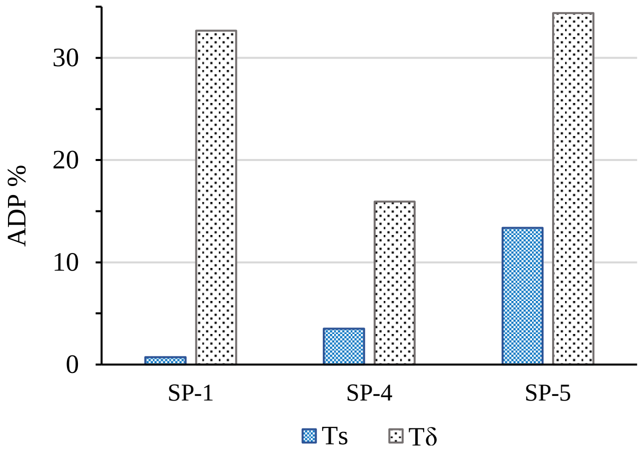


*Figure 5: Comparison of ADP % values of SP-1, SP-4 and SP-5 at two transition temperatures*

- **Types of damage and locations**

By studying the behaviour of SMPCs during programming, three types of damage were identified: (1) Type 1 - Internal fibre micro-buckling and debonding, (2) Type 2 - Delamination and (3) Type 3 - Through thickness cracking. Type 1 damage was observed at both temperatures $T_S$ and $T_\delta$, but only on the compressed side of the sample. Moreover, higher temperatures facilitated Type 1 damage due to the soften polymer matrix. Type 2 SMPC damage was also detected at both temperatures, mostly at the central region closer to the compressed side of the specimen. However, samples showed severe Type 2 damage at the higher temperature $T_\delta$. High SMP stiffness at the lower temperature $T_S$ resulted in Type 3 damage in samples with high thickness and fibre fraction. The chance of Type 3 damage increases at lower temperatures and it initiates at the tensioned side of the specimen. Of the three identified damage types, Types 1 and 2 were the most common as they occurred at both temperatures.

### 3.2.3 Taguchi optimization

Taguchi optimization can be carried out to maximize or minimize responses by the larger-the-better or the smaller-the-better criteria, respectively. For our application, maximizing almost all material parameters are favorable for SMPC performance. However, the ADP % damage quantifying factor should be minimized to achieve the best SMPC functionality. Therefore, a modified response $(1/ADP\ \%)_{MAX}$ was introduced as an alternative to $(ADP\ \%)_{MIN}$. Thus, by modifying the response for damage as 1/ADP, optimization analysis was easily carried out with the larger-the-better principle. Minitab 18 software was used to perform the Taguchi analysis and generate signal to noise (S/N) ratio plots.

- **For best overall material properties**

Taguchi optimization was also carried out for the test series considering $T_S$, $T_\delta$, $R_f$, $R_r$, 1/ADP %, $\sigma_T$, $E_T$, $\sigma_C$ and $E_C$ as responses to investigate most suitable SMPC parameters and achieve the best overall material properties (for both shape memory and mechanical). Table 6 presents the evaluated S/N ratios of the analysis, and the respective plot is given in Figure 6. Interestingly, the material parameters: glass fibre, 3 mm and 6 layers, were found to be the best constituents to achieve both shape memory and structural performance. Consequently, further tests included in this research were based on these selected SMPC parameters.

*Table 6: Response table for signal to noise ratios for overall SMPC performance considering $T_S$, $T_\delta$, $R_f$, $R_r$, 1/ADP, $\sigma_T$, $E_T$, $\sigma_C$ and $E_C$*

| **Level** | **Fibre type** | **Thickness** | **No of layers** |
|---|---|---|---|
| ***$T_S$, $T_\delta$, $R_f$, $R_r$, 1/ADP, $\sigma_T$, $E_T$, $\sigma_C$ and $E_C$: S/N ratios (Larger is better)*** | | | |
| 1 | -16.718 | -7.041 | -16.718 |
| 2 | -30.459 | -24.632 | -20.782 |
| 3 | -14.956 | -30.459 | -24.632 |
| Delta | 15.503 | 23.417 | 7.914 |
| Rank | 2 | 1 | 3 |

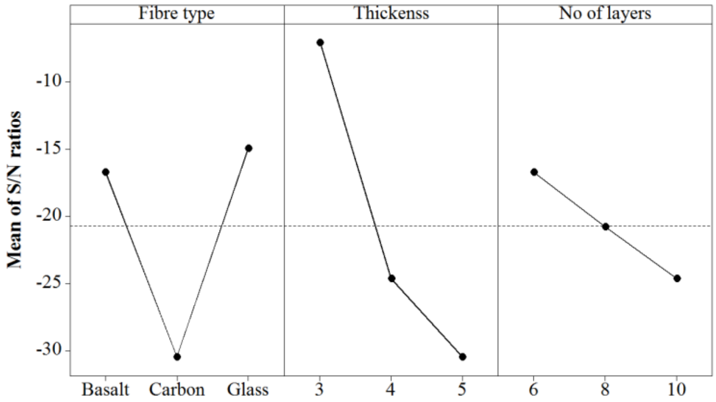


*Figure 6: S/N ratios of $T_S$, $T_\delta$, $R_f$, $R_r$, 1/ADP, $\sigma_T$, $E_T$, $\sigma_C$ and $E_C$ for overall SMPC performance*

### 3.3 Reinforcement modification

From the above Taguchi analysis, properties of specimens were optimized within the selected factors and levels. The analysis was done using the same reinforcement architecture in all tested samples. From this analysis, optimum material parameters were proposed to achieve the lowest possible damage level (but not ADP % = 0). However, even a minor damage level experienced in a programming stage could lead to a considerable drop in the material's mechanical properties and hinder performance of SMPC structural components. Therefore, having zero ADP % is mandatory for successful SMPC integrated applications. As a result, the fibre reinforcement architecture of the optimized SMPC was modified as a further refinement to enhance the SME without creating a reduction in strength. These further modifications aimed to achieve two objectives: (1) prevent any visible cracks (through thickness) and (2) ensure no change to the material's ultimate strength after shape programming. Two selected refinement strategies were implemented in order to achieve above mentioned objectives: (1) reinforcement orientation and architecture adjustment and (2) programming method parameter change. The optimum thickness of 3 mm and total number of layers (6 layers) were maintained along with the above refinements.

#### 3.3.1 Performance of two unidirectional fibres on either side (SP-10)

As explained in Section 3.2.2, to avoid the buckling or wrinkling of fibres, a new specimen (SP-10) was tested with unidirectional fibre layers placed on the outermost faces in the transverse direction, as illustrated in Figure 7. Then, the programming efficiency of the SP-10 sample was tested at $T_S$ and $T_\delta$. ADP % of SP-10 at $T_S$ and $T_\delta$ were calculated as 1.1 % and 19.6 %, respectively. As predicted, the damage level was lowest at $T_S$. Interestingly, sample SP-10 showed an outstanding improvement, with no damage on the compression side preventing formation of reinforcement wrinkles with micro-buckling. However, a few cracks were seen on the tension side of the bent SP-10 sample (as shown in

Figure 7). This can be attributed to the fibres oriented perpendicular to the tensile loads which created a directional weakness allowing SP-10 to crack on the tensioned side. Hence, SP-11 with only one unidirectional reinforcement on the compression side was fabricated and tested to achieve zero ADP %.

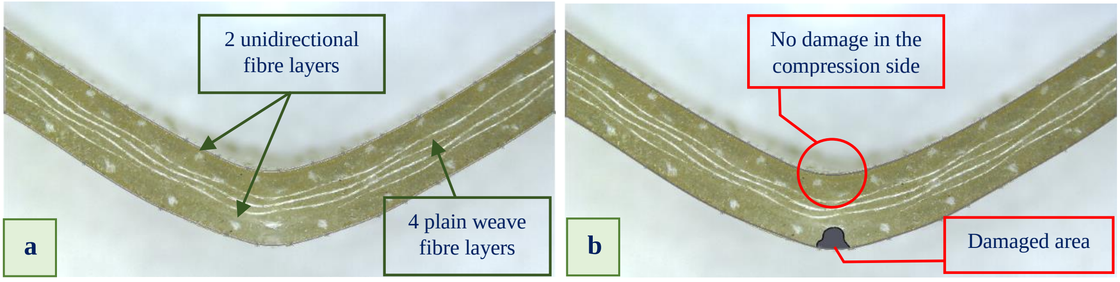


*Figure 7: Visible damage analysis of SP-10 with a reinforcement refinement (a) Deformed shape (b) Area of damage*

#### 3.3.2 Performance of unidirectional fibre on the compression side (SP-11)

Figure 8 shows a deformed SP-11 specimen with a unidirectional reinforcement layer positioned on the compression side of the sample. The remaining five layers did not change and were maintained as plain weave fabrics. According to the findings above, specimen SP-11 was programmed at the most effective temperature $T_S$. As depicted in Figure 8, a single unidirectional layer made a significant improvement in terms of damage resistance, and resulted a zero ADP %. Hence, visible damage (in Objective 1) was effectively prevented by means of appropriate adjustments in the reinforcement architecture. However, the SMPC should be able to retain its initial strength having gone through a complete shape memory thermomechanical cycle.

### 3.4 Evaluation of tensile properties after shape programming and recovery

#### 3.4.1 Tensile properties of SP-11

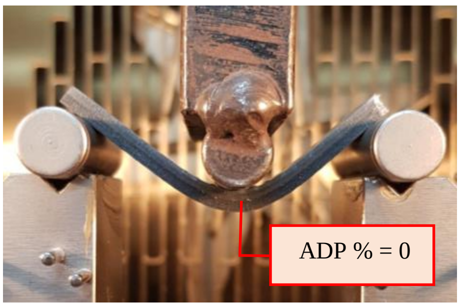


*Figure 8: Programming of SP-11 with no visible damage*

Tensile tests were carried out to evaluate the retained strength of the programmed and recovered samples. That is, to understand the impact of material programming on the structural characteristics of SMPCs. The stress (σ) – strain (ε) curves of programmed SMPCs after recovery and original sample are given in Figure 9. According to Taguchi optimization, basalt fibre was found to be the second best option for a low ADP % value. Hence, tensile test results of both glass and basalt SMPCs are included in Figure 9 for a comparison. Also, the same programming conditions used for the Taguchi damage and SME analysis were used in the shape training process of the SP-11 specimen. The notation “GL” and “B” stand for glass and basalt SMPCs.

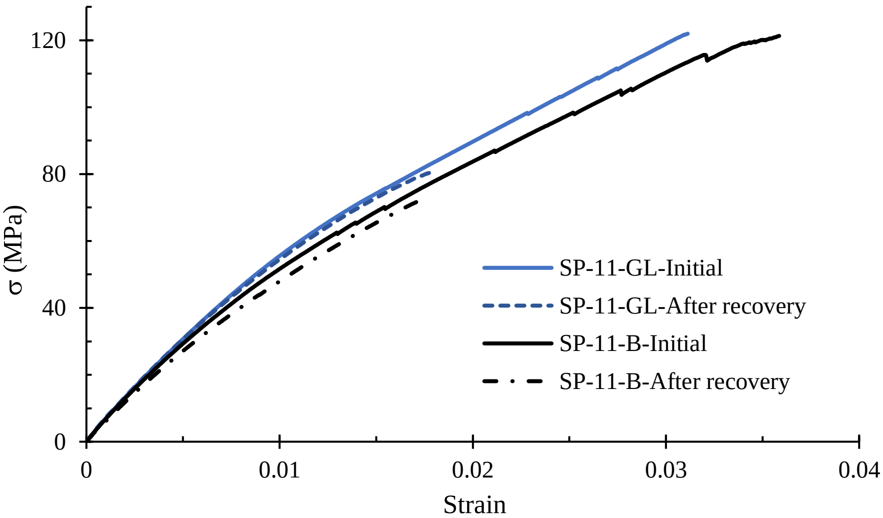


*Figure 9: Tensile σ-ε curves of glass and basalt SP-11 before and after programming*

As in Figure 9, both glass and basalt fibre composites showed similar properties and σ-ε behaviour under tensile loading. They also displayed an almost identical initial tensile strength of 122.9 MPa and 121.3 MPa respectively. Additionally, initial elastic moduli (E) were evaluated as 9.2 GPa and 9 GPa respectively for glass and basalt SMPCs. However, a drastic drop in tensile properties was observed in both programmed and recovered specimens. Table 7 gives a summary of the test results of both types of SMPCs before and after undergoing a complete thermomechanical cycle. The glass SMPC showed a 37 % and 10 % reduction in tensile strength and elastic modulus respectively. Moreover, the basalt SMPC experienced a 40 % and 18 % decline (σ and E) in tensile properties after programming. This can be attributed to internal minor loosening (Type 1) and separating of fibres (Type 2) due to a concentration of stress and loss of adhesion with the polymer matrix during SMPC programming. This phenomenon has reduced the amount of effective reinforcement in the SMPC which can withstand tensile loads, and hence resulted in a premature failure. Interestingly, reinforcement refinement minimized the severity of both Type 1 and 2 damage which had occurred at a small scale. Furthermore, these minor flaws were present between laminae inside the material which did not affect the visible damage quantifier ADP %. Hence, having a zero ADP % does not guarantee the perfect retainment of mechanical properties after recovery. Even though ADP % = 0 is mandatory to prevent visible cracks in the sample, identified minor flaws such as debonding between the fibres and matrix must be eliminated during the programming stage to avoid any decline in mechanical properties.

*Table 7: A summary of tensile test results of SP-11 samples before and after programming*

| SMPC | Initial | | After programming | | Reduction % | |
|---|---|---|---|---|---|---|
| | **σ (MPa)** | **E (GPa)** | **σ (MPa)** | **E (GPa)** | **Δσ %** | **ΔE %** |
| Glass | 122.9 | 9.2 | 78.0 | 8.3 | 37 | 10 |
| Basalt | 121.3 | 9 | 72.7 | 7.4 | 40 | 18 |

### 3.5 Programming method modification

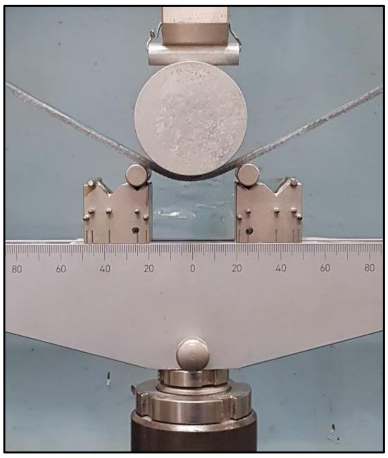


*Figure 10: Programming of SP-11-D50 with the refinement in programming process*

Stress concentrated in the bending region facilitated the debonding of fibres with the soft polymer matrix at the programming temperature. To achieve both ADP % = 0 and Δσ % = 0, a further refinement is required to eliminate internal fibre debonding and, hence, retain initial material structural properties. As the thickness of SMPC is constant throughout the sample, stress concentration can only be reduced through an adjustment to programming process parameters. Increasing the support span or bend radius of the specimen will help to distribute bending stresses throughout the sample, allowing it to deform easily with minimal internal damage. Figure 10 illustrates the adjusted programming process with a 50 mm (five folds higher than previous) diameter deforming tool. Figure 12 presents σ-ε curves of glass and basalt SMPCs programmed under the modified process and named as "D50". Most importantly, recovered samples showed an almost identical tensile strength as their initial properties. Both composites displayed a negligible decline in tensile strength of 0.9 % and 0.1 %. Moreover, the strain at break of both SMPCs increased, proving an improvement in material elasticity. The decline in elastic modulus also showed an improvement compared to the previous tests, however recovered glass and basalt fibre composites showed 9 % and 10 % modulus reduction respectively. The existence of a few locations with minor Type 1 damage with internal fibre debonding (as in Figure 11 (c)) caused this slight drop in modulus. This claim has been validated numerically with the help of the developed FEA approach (discussed in Section 4). In addition, the increased elasticity of the material adversely affected the reduction in elastic modulus of the SMPCs. Figure 11 depicts a deformed glass SMPC with new programming process parameters. Table 8 and Figure 13 present a summary of the evaluated results and clearly demonstrate significant improvement in SMPC performance even after shape recovery. With the refinements introduced, both visible damage level and strength drop could be mitigated which will eventually enhance SMPC performance in future prospective applications.

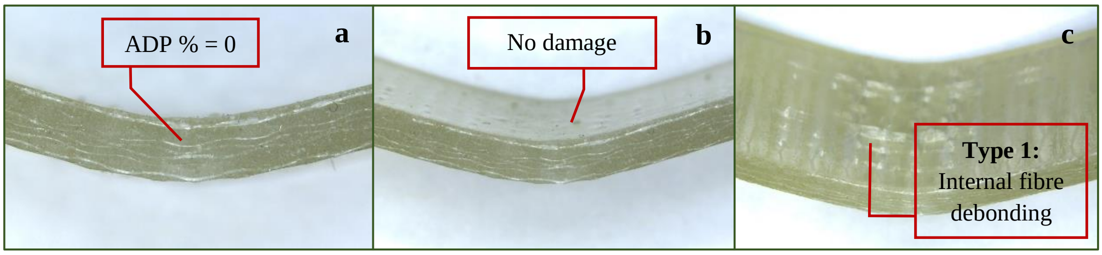


*Figure 11: SP-11-GL-D50 sample photographs after programming*

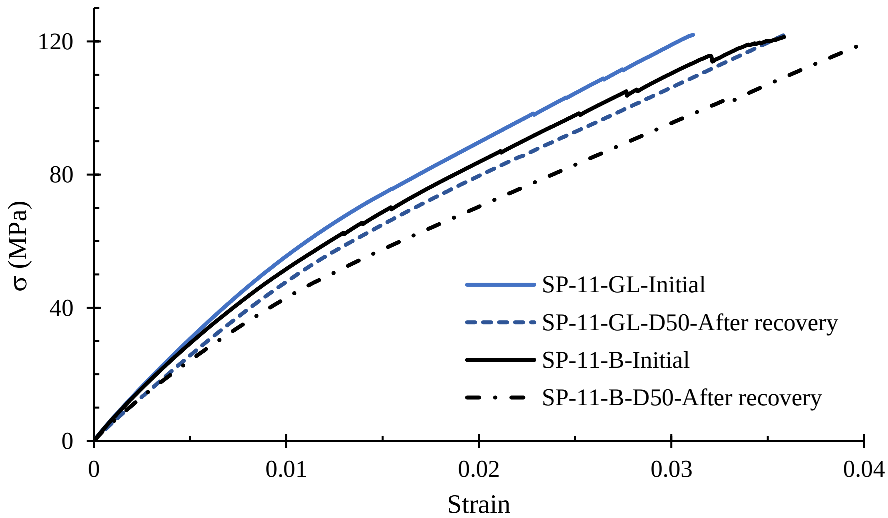


*Figure 12: Tensile $\sigma$-$\varepsilon$ curves of glass and basalt SP-11-D50 before and after programming*

*Table 8: A summary of tensile test results of SP-11-D50 samples before and after programming*

| SMPC | Initial | | After programming | | Reduction % | |
|---|---|---|---|---|---|---|
| | **σ (MPa)** | **E (GPa)** | **σ (MPa)** | **E (GPa)** | **Δσ %** | **ΔE %** |
| Glass | 122.9 | 9.2 | 121.8 | 8.4 | 0.9 | 9 |
| Basalt | 121.3 | 9 | 121.2 | 8.1 | 0.1 | 10 |

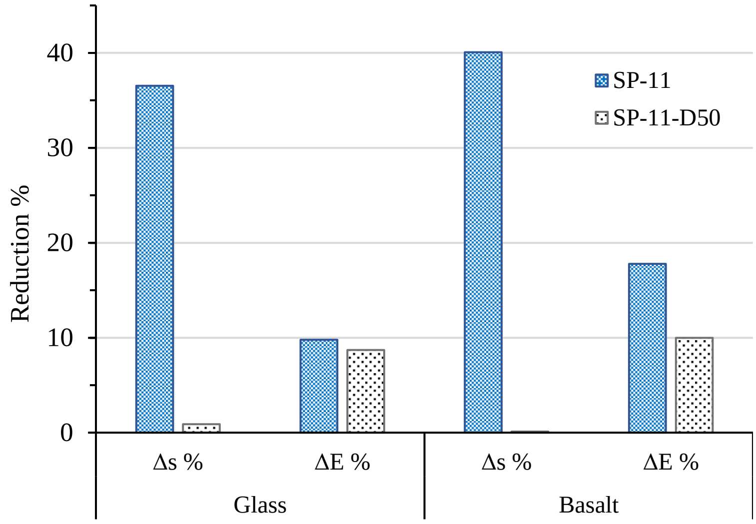


*Figure 13: Comparison of reductions in tensile strength and modulus of SP-11 and SP-11-D50 glass and basalt SMPCs*

## 4. Numerical validation of experimental results

### 4.1 Validation of results via ABAQUS FEA model

A numerical simulation was implemented in ABAQUS to investigate induced stress distribution in the optimized SMPC during the programming stage and develop a damage prediction strategy. In keeping with the scope of the article, only the programming stage of SMPCs is analyzed here. Figure 14 presents the modelled assembly with initial and programmed shapes. Experimental results (load versus time) extracted from the MTS 10 kN testing equipment and calculated flexural stress during the programming stage of SP-11 were used to validate the FEA approach implemented in ABAQUS. Figure 16(a) and (b) show the comparison of the maximum flexural stress magnitude and load due to the programming of the glass sample SP-11-GL. The curves fit perfectly until Point 1 (Figure 16) where the Type 1 SMPC damage begins. Type 1 damage developed until a displacement of 7 mm (Point 2) where Type 2 damage occurred, further reducing the load. Hence, by matching this scenario, CSMs can be introduced to predict the occurrence of Types 1 and 2 damage from FEA results.

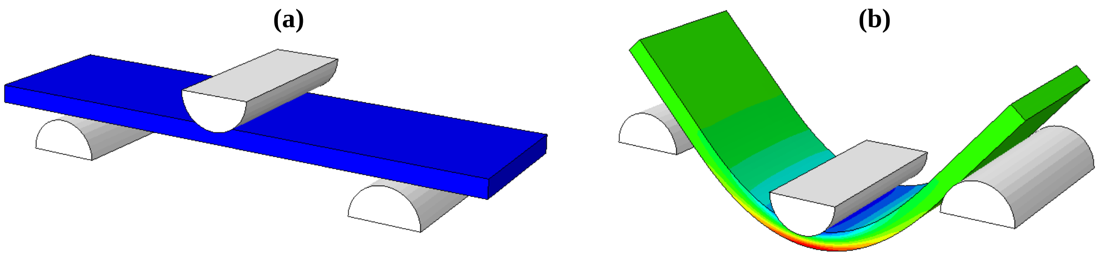


*Figure 14: Shape programming in ABAQUS (a) Initial shape (b) Programmed shape*

Most importantly, for the best SMPC performance, a zero damage level is mandatory. Thus, a numerical analysis should be developed to predict $\sigma_o$ which can then be used as a tool to predict whether damage in the programming stage is likely or not. Hence, it can be concluded that $\sigma_o$ as the most critical factor for SMPC programming.  As the model does not take into account the behaviour of post damage, interfacial bond properties and progressive failure of SMPCs, FEA results do not match with the experimental data beyond Point 1. However, if needed, properties of the nanoscale matrix-fibre interface and mechanics of stress transfer can be analyzed using shear lag theory and traction-separation law as previously studied by Budurapu et al (2019) [45] and Skovsgaard et al (2021) [46]. This analysis is not included here as it is not within the scope of the article.

Therefore, a compressive stress of 70 MPa (= $\sigma_o$) should not be exceeded during programming to avoid all types of damages at $T_S$. Thus, the interfacial bond strength of the SMPC can also be described as 70 MPa [41]. Moreover, stress values from 70 MPa to 100 MPa will cause Type 1 damage, and Type 2 damage will develop beyond 100 MPa (given in Figure 17). Hence, the selected CSM facilitates prompt prediction of programming effectiveness of the SMPC, enables selection of the most suitable programming parameters through FEA, and saves time. Figure 18 illustrates the FEA stress results of the SP-11-GL-D50 with 60 mm span described in Section 3.5. According to the proposed CSM, it is evident that the SMPC reached the Type 1 damage region which resulted a decline in modulus. However, as the maximum stress is well below the Type 2 region, no change in strength can be expected. The respective FEA results of SP-11 and SP-11-GL-D50 are given in Figure 15, where $S_{11}$ = $S_{xx}$ = flexural stress. These FEA results and damage predictions validate the experimental observations and outcomes which can be effectively applied in future SMPC developments.

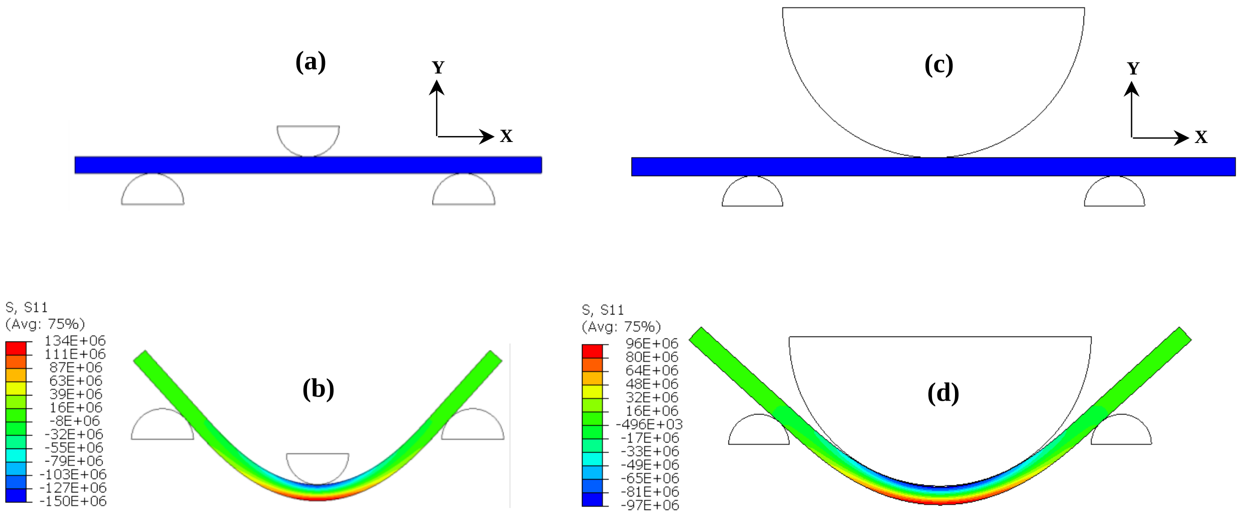


*Figure 15: Stress variation of programmed samples (a) SP-11 before programming (b) Programmed SP-11 (c) SP-11-D50 before programming (d) Programmed SP-11-D50*

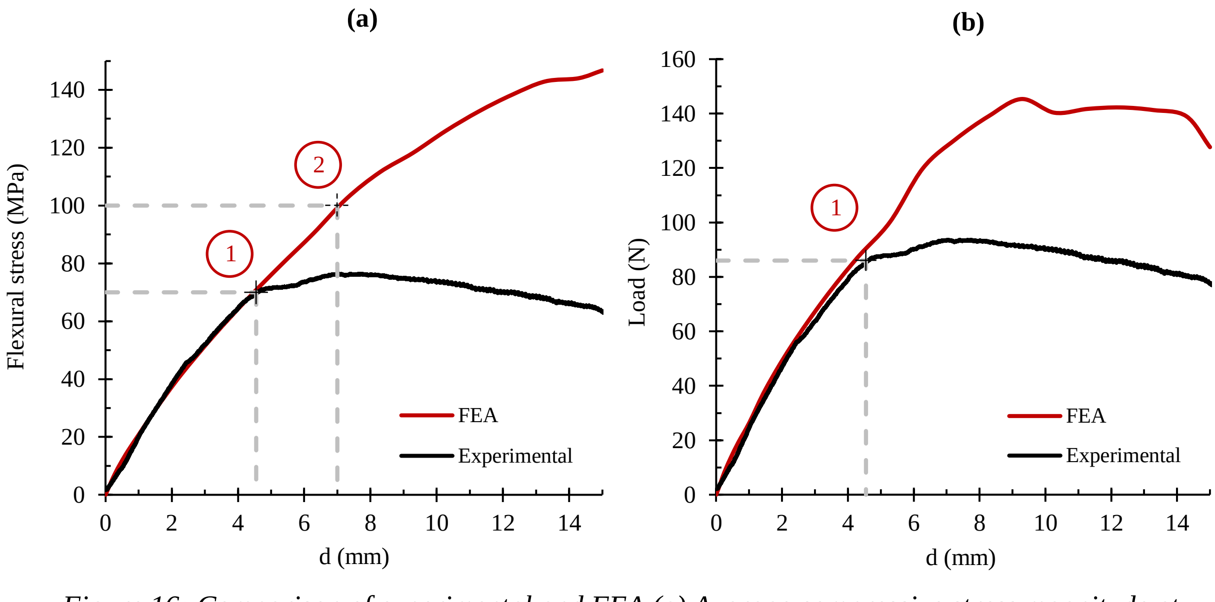


*Figure 16: Comparison of experimental and FEA (a) Average compressive stress magnitude at the most critical location of the SMPC (b) Applied load for programming*

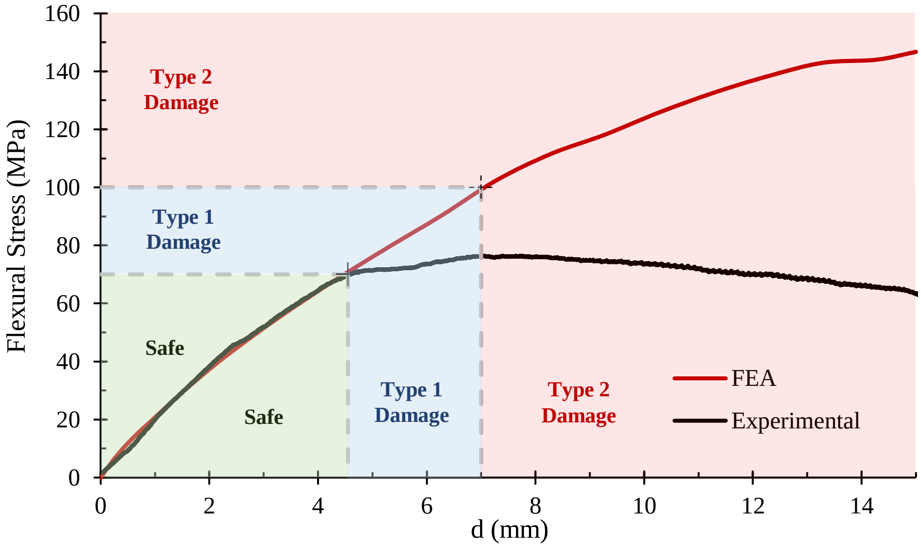


*Figure 17: Critical stress margins introduced to predict programming effectiveness through FEA*

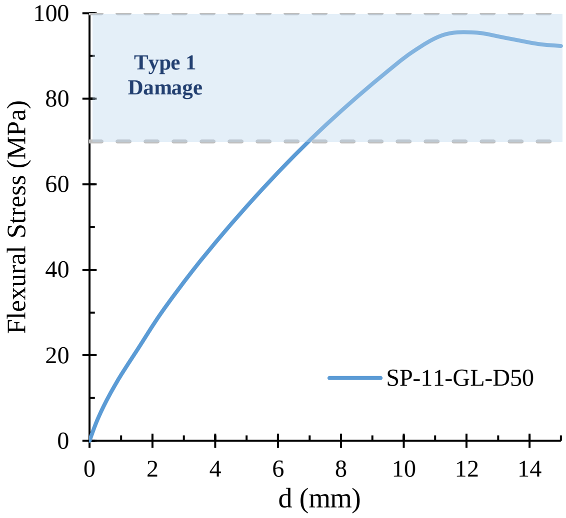


*Figure 18: FEA stress results for the shape programming process of SP-11-GL with 50 mm bend diameter*

## 5. Conclusion

A novel user-friendly approach to quantify damage has been introduced and implemented in this research to identify damage incorporated in SMPCs during shape programming. It was revealed that high SMPC thickness and reinforcement content adversely affects the effectiveness of the shape programming process, resulting in material flaws. A new dimensionless quantity (ADP %) has been introduced and can be used by researchers as a user friendly through thickness visible damage quantifier in SMPCs when programming. A robust Taguchi L9 array was implemented to achieve the lowest ADP % along with the best possible mechanical properties. Further, two refinements in the reinforcement architecture and programming process were proposed and tested to achieve ADP % = 0 and no decline in ultimate tensile strength ($\Delta\sigma = 0$ %). From the analysis, three types of SMPC damage were identified and the material's compression side was also identified as the most critical location susceptible to damage while programming. The best programming characteristics for optimum performance were shown at the low temperature $T_S$ (~ 60 °C) coupled with a higher deformation rate (60 mm/min). The best combination of SMPC material parameters was evaluated as glass fibre reinforcement, 3 mm and 6 layers (5 plain weave + 1 unidirectional layer on the compression side with fibres in the transverse direction). In addition, experimental results were validated using FEA analysis and CSM guidelines were proposed to predict possible damage levels during programming. Hence, 70 MPa was found to be the $\sigma_o$ or interfacial bond strength of the optimized glass SMPC to undergo perfect programming. Overall, the study provides first hand comprehensive programming damage investigation of SMPCs including a novel experimental and numerical framework to optimize and design SMPC integrated structural components for future constructions.

## 6. References


[1] A. Lendlein and S. Kelch, "Shape-Memory Polymers," *Angewandte Chemie International Edition*, vol. 41, no. 12, pp. 2034-2057, 2002, doi: 10.1002/1521-3773(20020617)41:12<2034::Aid-anie2034>3.0.Co;2-m.

[2] Q. Meng and J. Hu, "A review of shape memory polymer composites and blends," *Composites Part A: Applied Science and Manufacturing,* vol. 40, no. 11, pp. 1661-1672, 2009, doi: 10.1016/j.compositesa.2009.08.011.

[3] L. Sun *et al.*, "Stimulus-responsive shape memory materials: A review," *Materials & Design,* vol. 33, pp. 577-640, 2012, doi: 10.1016/j.matdes.2011.04.065.

[4] W. Al Azzawi, M. M. Islam, J. Leng, F. Li, and J. A. Epaarachchi, "Quantitative and qualitative analyses of mechanical behavior and dimensional stability of styrene-based shape memory composites," *Journal of Intelligent Material Systems and Structures,* vol. 28, no. 20, pp. 3115-3126, 2017, doi: 10.1177/1045389x17705210.

[5] S. Madbouly and A. Lendlein, "'Shape Memory Polymer Composites'," in *Advanced Polymer Science*: Springer-Verlag Berlin Heidelberg, 2009, pp. 1-55.

[6] W. Al Azzawi, M. Herath, and J. Epaarachchi, "Modeling, analysis, and testing of viscoelastic properties of shape memory polymer composites and a brief review of their space engineering applications," *Creep and Fatigue in Polymer Matrix Composites,* pp. 465-495, 2019.

[7] H. M. C. M. Herath, J. A. Epaarachchi, M. M. Islam, W. Al-Azzawi, J. Leng, and F. Zhang, "Structural performance and photothermal recovery of carbon fibre reinforced shape memory polymer," *Composites Science and Technology,* vol. 167, pp. 206-214, 2018, doi: 10.1016/j.compscitech.2018.07.042.

[8] L. Tan, L. Gan, J. Hu, Y. Zhu, and J. Han, "Functional shape memory composite nanofibers with graphene oxide filler," *Composites Part A: Applied Science and Manufacturing,* vol. 76, pp. 115-123, 2015.

[9] Y. Liu, H. Lv, X. Lan, J. Leng, and S. Du, "Review of electro-active shape-memory polymer composite," *Composites Science and Technology,* vol. 69, no. 13, pp. 2064-2068, 2009.

[10] J. Leng, H. Lv, Y. Liu, and S. Du, "Synergic effect of carbon black and short carbon fiber on shape memory polymer actuation by electricity," *Journal of Applied Physics,* vol. 104, no. 10, p. 104917, 2008.

[11] M. Herath, J. Epaarachchi, M. Islam, C. Yan, F. Zhang, and J. Leng, "Effects of selectively triggered photothermal particles on shape memory polymer composites: An investigation on structural performance, thermomechanical characteristics and photothermal behaviour," *Journal of Intelligent Material Systems and Structures,* vol. 30, no. 20, pp. 3124-3135, 2019.

[12] T. Ohki, Q.-Q. Ni, N. Ohsako, and M. Iwamoto, "Mechanical and shape memory behavior of composites with shape memory polymer," *Composites Part A: Applied Science and Manufacturing,* vol. 35, no. 9, pp. 1065-1073, 2004, doi: 10.1016/j.compositesa.2004.03.001.

[13] X. Lan, Y. Liu, H. Lv, X. Wang, J. Leng, and S. Du, "Fiber reinforced shape-memory polymer composite and its application in a deployable hinge," *Smart Materials and Structures,* vol. 18, no. 2, p. 024002, 2009.

[14] P. Keller *et al.,* "Development of a deployable boom for microsatellites using elastic memory composite material," in *45th AIAA/ASME/ASCE/AHS/ASC Structures, Structural Dynamics & Materials Conference*, 2004, p. 1603.

[15] J. Lin, C. Knoll, and C. Willey, "Shape memory rigidizable inflatable (RI) structures for large space systems applications," in *47th AIAA/ASME/ASCE/AHS/ASC*

*Structures, Structural Dynamics, and Materials Conference 14th AIAA/ASME/AHS Adaptive Structures Conference 7th*, 2006, p. 1896.
[16] P. Yang, "Research on the structure of space deployable antenna based on shape memory polymer composites," Dissertation for the Master Degree in Engineering, School of Astronautic …, 2011.
[17] W. Yin, T. Fu, J. Liu, and J. Leng, "Structural shape sensing for variable camber wing using FBG sensors," in *Sensors and Smart Structures Technologies for Civil, Mechanical, and Aerospace Systems 2009*, 2009, vol. 7292: International Society for Optics and Photonics, p. 72921H.
[18] J. Lin, H. Fang, E. Im, and U. Quijano, "Concept study of a 35-m spherical reflector system for NEXRAD in space application," in *47th AIAA/ASME/ASCE/AHS/ASC Structures, Structural Dynamics, and Materials Conference 14th AIAA/ASME/AHS Adaptive Structures Conference 7th*, 2006, p. 1604.
[19] H. Du, L. Liu, J. Leng, H. Peng, F. Scarpa, and Y. Liu, "Shape memory polymer S-shaped mandrel for composite air duct manufacturing," *Composite Structures*, vol. 133, pp. 930-938, 2015.
[20] W. Ferdous, Y. Bai, T. D. Ngo, A. Manalo, and P. Mendis, "New advancements, challenges and opportunities of multi-storey modular buildings – A state-of-the-art review," *Engineering Structures*, vol. 183, pp. 883-893, 2019, doi: 10.1016/j.engstruct.2019.01.061.
[21] H.-T. Thai, T. Ngo, and B. Uy, "A review on modular construction for high-rise buildings," *Structures*, vol. 28, pp. 1265-1290, 2020, doi: 10.1016/j.istruc.2020.09.070.
[22] H. M. C. M. Herath, J. A. Epaarachchi, M. M. Islam, and J. Leng, "Carbon Fibre Reinforced Shape Memory Polymer Composites for Deployable Space Habitats," *Engineer: Journal of the Institution of Engineers, Sri Lanka*, vol. 52, no. 1, 2019, doi: 10.4038/engineer.v52i1.7323.
[23] X. Lan, L. Liu, Y. Liu, J. Leng, and S. Du, "Post microbuckling mechanics of fibre-reinforced shape-memory polymers undergoing flexure deformation," *Mechanics of Materials*, vol. 72, pp. 46-60, 2014.
[24] K. Gall, M. Mikulas, N. A. Munshi, F. Beavers, and M. Tupper, "Carbon fiber reinforced shape memory polymer composites," *Journal of intelligent material systems and structures*, vol. 11, no. 11, pp. 877-886, 2000.
[25] J. Gu, J. Leng, H. Sun, H. Zeng, and Z. Cai, "Thermomechanical constitutive modeling of fiber reinforced shape memory polymer composites based on thermodynamics with internal state variables," *Mechanics of Materials*, vol. 130, pp. 9-19, 2019, doi: 10.1016/j.mechmat.2019.01.004.
[26] J. Gu, H. Zeng, Z. Cai, and H. Sun, "Modeling the laminated carbon fiber reinforced shape memory polymer composites by using a refined plate theory," *Smart Materials and Structures*, vol. 29, no. 9, 2020, doi: 10.1088/1361-665X/ab9e08.
[27] T. Xie and I. A. Rousseau, "Facile tailoring of thermal transition temperatures of epoxy shape memory polymers," *Polymer*, vol. 50, no. 8, pp. 1852-1856, 2009, doi: 10.1016/j.polymer.2009.02.035.
[28] W. A. Azzawi, J. A. Epaarachchi, M. Islam, and J. Leng, "Implementation of a finite element analysis procedure for structural analysis of shape memory behaviour of fibre reinforced shape memory polymer composites," *Smart Materials and Structures*, vol. 26, no. 12, 2017, doi: 10.1088/1361-665X/aa928e.
[29] G. Li and A. Wang, "Cold, warm, and hot programming of shape memory polymers," *Journal of Polymer Science Part B: Polymer Physics*, vol. 54, no. 14, pp. 1319-1339, 2016, doi: 10.1002/polb.24041.

[30] K. Shahi, R. Boomurugan, and R. Velmurugan, "Cold programming of epoxy-based shape memory polymer," *Structures*, vol. 29, pp. 2082-2093, 2021, doi: 10.1016/j.istruc.2020.05.023.
[31] D. M. Feldkamp and I. A. Rousseau, "Effect of the deformation temperature on the shape-memory behavior of epoxy networks," *Macromolecular Materials and Engineering*, vol. 295, no. 8, pp. 726-734, 2010.
[32] Y. Liu, C. Han, H. Tan, and X. Du, "Thermal, mechanical and shape memory properties of shape memory epoxy resin," *Materials Science and Engineering: A*, vol. 527, no. 10-11, pp. 2510-2514, 2010, doi: 10.1016/j.msea.2009.12.014.
[33] K. Emmanuel, H. Herath, L. Jeewantha, J. Epaarachchi, and T. Aravinthan, "Thermomechanical and fire performance of DGEBA based shape memory polymer composites for constructions," *Construction and Building Materials*, vol. 303, p. 124442, 2021.
[34] L. Jeewantha, K. Emmanuel, H. Herath, M. Islam, L. Fang, and J. Epaarachchi, "Multi-attribute parametric optimisation of shape memory polymer properties for an adaptive orthopaedic plasters," *Materialia*, p. 101325, 2022.
[35] Y. C. Wang and V. Kodur, "Variation of strength and stiffness of fibre reinforced polymer reinforcing bars with temperature," *Cement and Concrete Composites*, vol. 27, no. 9-10, pp. 864-874, 2005.
[36] G. Yang, M. Park, and S.-J. Park, "Recent progresses of fabrication and characterization of fibers-reinforced composites: A review," *Composites Communications*, vol. 14, pp. 34-42, 2019, doi: 10.1016/j.coco.2019.05.004.
[37] P. Amuthakkannan, V. Manikandan, J. W. Jappes, and M. Uthayakumar, "Effect of fibre length and fibre content on mechanical properties of short basalt fibre reinforced polymer matrix composites," *Materials physics and mechanics*, vol. 16, no. 2, pp. 107-117, 2013.
[38] H. Ku, H. Wang, N. Pattarachaiyakoop, and M. Trada, "A review on the tensile properties of natural fiber reinforced polymer composites," *Composites Part B: Engineering*, vol. 42, no. 4, pp. 856-873, 2011.
[39] R. Rahman and S. Z. F. S. Putra, "Tensile properties of natural and synthetic fiber-reinforced polymer composites," *Mechanical and physical testing of biocomposites, fibre-reinforced composites and hybrid composites*, pp. 81-102, 2019.
[40] J. Liu, L. Xiang, and T. Kan, "The effect of temperature on the bending properties and failure mechanism of composite truss core sandwich structures," *Composites Part A: Applied Science and Manufacturing*, vol. 79, pp. 146-154, 2015, doi: 10.1016/j.compositesa.2015.09.017.
[41] H. Aglan, Z. Qian, and D. Mitra-Majumdar, "The effect of temperature on the critical failure properties of advanced polymer composites," *Polymer testing*, vol. 11, no. 3, pp. 169-184, 1992.
[42] D. Li, D. Fang, G. Zhang, and H. Hu, "Effect of temperature on bending properties and failure mechanism of three-dimensional braided composite," *Materials & Design*, vol. 41, pp. 167-170, 2012, doi: 10.1016/j.matdes.2012.04.055.
[43] C. Shenghu, W. Xin, and W. Zhishen, "Evaluation and prediction of temperature-dependent tensile strength of unidirectional carbon fiber-reinforced polymer composites," *Journal of Reinforced Plastics and Composites*, vol. 30, no. 9, pp. 799-807, 2011, doi: 10.1177/0731684411411002.
[44] Z. Jia, T. Li, F.-p. Chiang, and L. Wang, "An experimental investigation of the temperature effect on the mechanics of carbon fiber reinforced polymer composites," *Composites Science and Technology*, vol. 154, pp. 53-63, 2018, doi: 10.1016/j.compscitech.2017.11.015.

[45] P. R. Budarapu, S. Kumar, B. G. Prusty, and M. Paggi, "Stress transfer through the interphase in curved-fiber pullout tests of nanocomposites," *Composites Part B: Engineering*, vol. 165, pp. 417-434, 2019, doi: 10.1016/j.compositesb.2018.12.116.
[46] S. P. H. Skovsgaard and S. Heide-Jørgensen, "Three-dimensional mechanical behavior of composite with fibre-matrix delamination through homogenization of micro-structure," *Composite Structures*, vol. 275, 2021, doi: 10.1016/j.compstruct.2021.114418.